Check for updates

A simple multiple centrifugation method for large-area homogeneous perovskite CsPbBr₃ films with optical lasing†

Chang-Gui Lu,‡* Xue-Fang Hu,‡ Shu-Hong Xu, [iD] Hong-Gui Liu, Jing-Kun Xu, Yi-Ping Cui [iD] and Chun-Lei Wang [iD]*

Large scale cesium lead-halide (CsPbX₃, X = Cl, Br, and I) perovskite films have become the basis of laser applications. Common fabrication methods such as spin-coating and thermal evaporation have a trade-off between high quality and low cost. Herein, we reported a facile method for preparing a large area homogeneous perovskite CsPbBr₃ film *via* a multiple centrifugal deposition and solvent annealing (MCDSA) method. This method is superior because it can control the thickness (180 nm to 880 nm) of the film, ensure the film is crack and pinhole free, has a large area (2.5 cm × 2.5 cm), and has a low surface roughness (a root mean square of 32 nm). Multiple times of centrifugation and solvent annealing in the MCDSA method are key to improving the quality of the film as well as the laser performance. With increased centrifugation cycles from one to four, the thickness of the film increases from 180 nm to 880 nm, leading to a decrease in the laser threshold from 18.1 μJ cm^{-2} to 14.2 μJ cm^{-2} and an increase in the gain coefficient from 78.5 cm^{-1} to 112.7 cm^{-1}. When solvent annealing is employed, the gain coefficient is further increased to 122.7 cm^{-1}.

1 Introduction

Recently, all-inorganic cesium lead-halide (CsPbX₃, X = Cl, Br, and I) perovskite films have grown in popularity due to their superior optical properties such as high photoluminescence quantum yields (PLQYs),[1,2] narrow emission line widths,[3,4] wide emission spectra tunability,[5–7] and low material costs.[8,9] These properties make them a prime candidate for use in solar cells,[10–12] white light-emitting diodes,[13–15] displays,[16] photodetectors,[17,18] laser and so on.[19–21] The fabrication of high quality CsPbX₃ perovskite films is a prerequisite for numerous applications. For example in laser applications, perovskite films act as the gain medium and the resonant cavity. The film quality, including its smoothness, the homogeneousness of its large area, and thickness, are fundamental for realizing low threshold and high gain coefficients.

There are numerous ways to fabricate CsPbBr₃ films. The most common methods are spin-coating and thermal evaporation. Spin-coating is a facile preparation approach, which is achieved by dropping a CsPbBr₃ solution onto the substrate while rotating at a high speed. Thus, making this method very easy to operate. The as-prepared CsPbBr₃ films usually result in inhomogeneous samples (having numerous cracks and uncovered pin-holes) with relatively large surface roughness. Moreover, this method wastes a serious amount of material, almost 99% of the source is out of use, making it unsuitable for mass production. Since spin-coating does not deposit compact and homogeneous films with large areas, numerous post-treatments are necessary to improve the morphology and crystallinity of the films.[22–25] Thermal evaporation is another effective way to fabricate large-scale CsPbBr₃ films. In this method, the source material is placed in an evaporator and the high temperature deposits the source material on the substrate, making the film compact and homogeneous over a large area. In comparison to spin-coating, the thermal evaporation method can produce CsPbBr₃ films with better crystalline qualities, lower defect densities, and highly flat and smooth surfaces. In particular, thermal evaporation has shown great success in creating high-quality nanostructures with controllable thickness. However, the synthesis process is complicated and requires dedicated equipment. Designated experimental conditions are also needed, leading to increased costs of the films.[26–30] Overall, both spin-coating and thermal evaporation do not satisfy the requirement of high quality and low cost simultaneously. Thus, it is highly desirable to develop a new method that aims to produce CsPbBr₃ films with good surface characteristics in an inexpensive manner.

In this study, we develop a multiple centrifugal deposition and solvent annealing (MCDSA) method for the large scale

Advanced Photonics Center, School of Electronic Science & Engineering, Southeast University, Nanjing, Jiangsu, 210096, China. E-mail: changguilu@seu.edu.cn; wangchl@seu.edu.cn

† Electronic supplementary information (ESI) available. See DOI: 10.1039/d0ra04259e
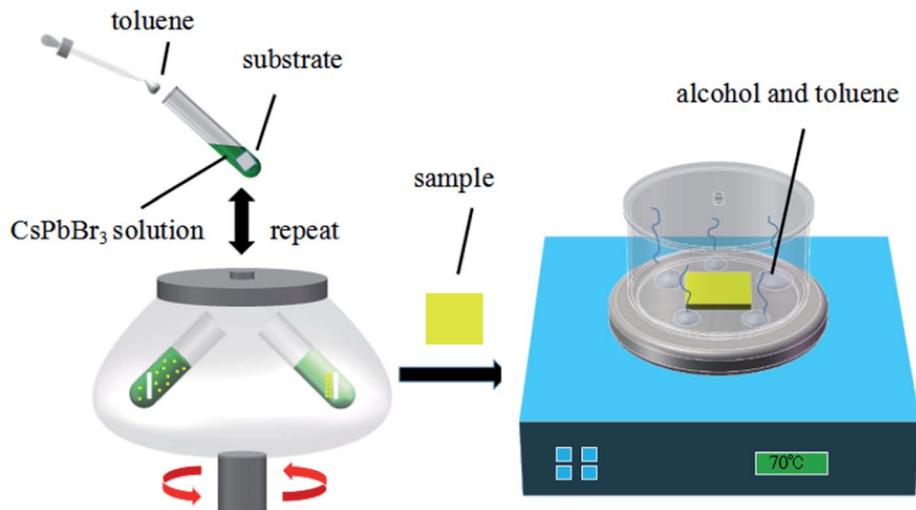
‡ These authors contributed equally to this work.

Fig. 1 The flow diagram of the MCDSA method.

fabrication of $CsPbBr_3$ films with low surface roughness, low cost and good stability.[31–34] By changing the repetition times of the centrifugation process, the thickness of the $CsPbBr_3$ films can be controlled. Due to the high quality of the films, with a low surface roughness (root mean square of 32 nm) and a large area (2.5 cm × 2.5 cm), the as-prepared $CsPbBr_3$ films show good laser performance. The measured ASE threshold and the gain coefficient are 14.2 μJ cm^{-2} and 122.7 cm^{-1}, respectively. We note the recent report of colloidal quantum dot films fabricated using a centrifugal casting method.[35,36] Though the films are crack-free and macroscopically uniform over large areas, the films are thin, making them only suitable for photodetector rather than laser applications. Thus, this work is the first report of a simple preparation and low cost method for obtaining $CsPbBr_3$ films with large area homogeneity, a low laser threshold, and a high gain coefficient, which has promising applications in the optical lasing field.

2 Results and discussion

2.1 Preparation of $CsPbBr_3$ films

Fig. 1 illustrates the typical MCDSA method, which includes three steps: (1) the preparation of $CsPbBr_3$ quantum dots (QDs) by mixing toluene with a dimethylsulfoxide (DMSO) solution
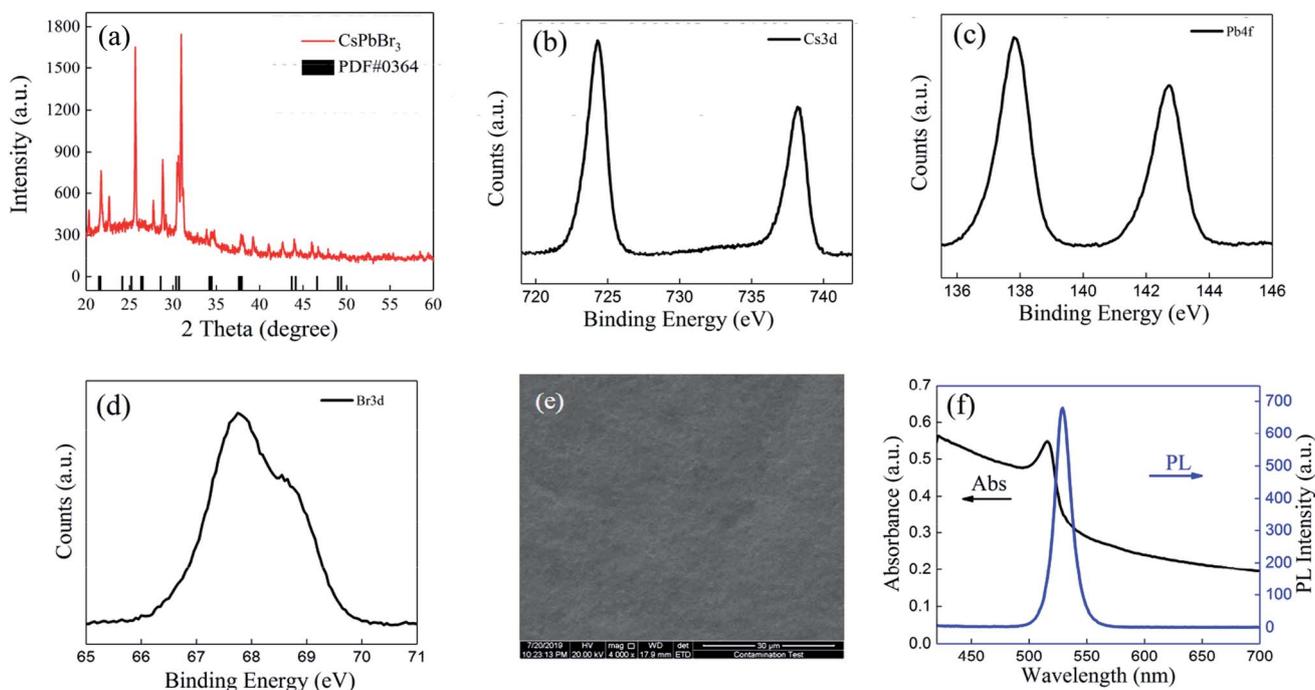

Fig. 2 (a) The XRD pattern of the $CsPbBr_3$ film. (b) High-resolution XPS spectra of Cs3d, (c) Pb4f, and (d) Br3d. (e) SEM image. (f) The PL intensity and absorption of the $CsPbBr_3$ film.
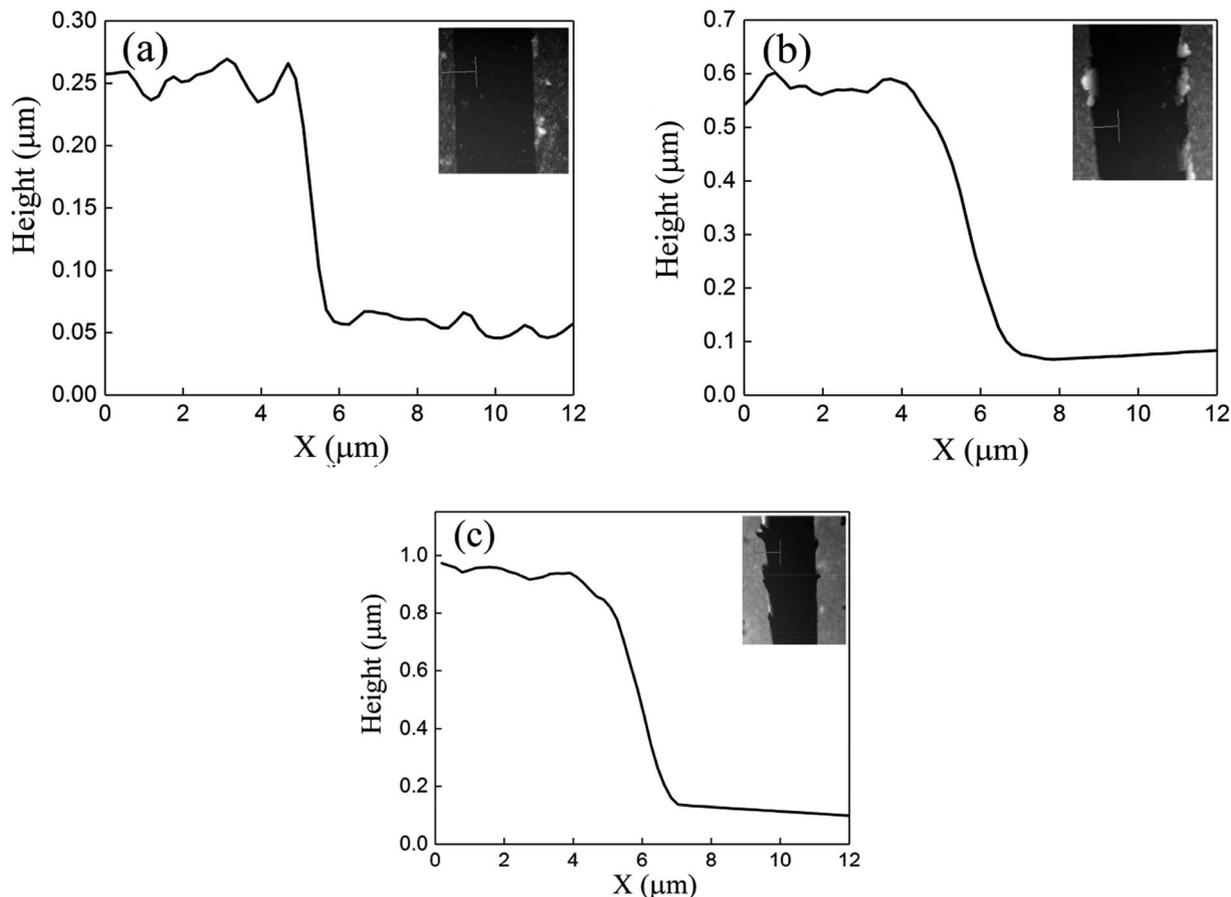
Fig. 3 The AFM pattern of the CsPbBr$_3$ films (a) S$_A$, (b) S$_B$, and (c) S$_C$.

containing oleic acid (OA), oleylamine (OAm), CsBr, and PbBr$_2$; (2) multiple times of centrifugation by putting the substrate in a freshly prepared CsPbBr$_3$ QD solution; (3) solvent-gas atmosphere annealing by putting the substrate in a closed cuvette surrounded by alcohol and toluene vapors (see details in the ESI†).

X-ray diffraction (XRD) of the CsPbBr$_3$ perovskite film in N$_2$ atmosphere was recorded and is shown in Fig. 2(a). The strong intensity of the diffraction peaks indicates the good crystallinity of the film. Most of the peaks are in agreement with the standard (rhombic) CsPbBr$_3$ (PDF#18-0364). The XRD pattern of the CsPbBr$_3$ perovskite film in an air atmosphere was also measured. The presence of PbBr$_2$ proved that an incomplete reaction occurred during the fabrication process (Table S2 in ESI†). A stability test conducted on the PL intensity indicated

that the PL intensity is stable if stored in a N$_2$ atmosphere rather than an air atmosphere (Table S3 in ESI†). The X-ray photoelectron spectroscopy (XPS) results shown in Fig. 2(b)–(d) display typical Cs peaks at 724.3 and 738.2 eV, Pb peaks at 137.9 and 142.7 eV and the Br peaks at 67.7 and 68.8 eV. From the SEM image in Fig. 2(e), we can see that the film is homogeneous and compact over a large area. No pinholes can be found. The absorption/photoluminescence (PL) spectrum of the CsPbBr$_3$ films (Fig. 2(f)) displays an obvious peak at 516/529 nm, which is similar to that of the CsPbBr$_3$ QD solution shown in Fig. S1 in the ESI†.

One advantage of the MCDSA method is its ability to control the thickness of the film simply by changing the number of centrifugation steps. Three samples (labeled S$_A$, S$_B$, and S$_C$) were fabricated using the MCDSA method with repetition numbers of
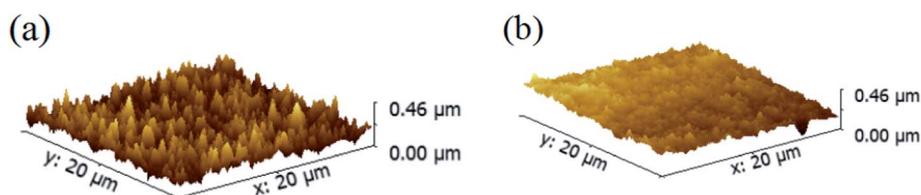

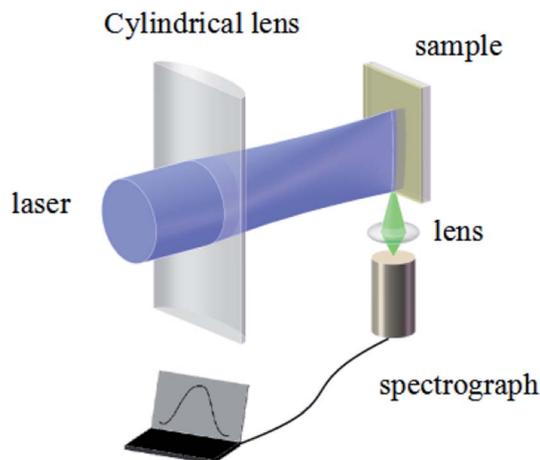Fig. 4 The AFM pattern of the CsPbBr$_3$ film S$_A$ (a) direct annealing (b) solvent annealing.

Fig. 7 (a) The ASE intensity of the S_C sample *versus* the intensity of the pump laser. (b) The PL intensity of the S_C sample *versus* the excitation length.

The output divergence angle after collimation is approximately 0.65 mrad. Using a beta barium borate (BBO) crystal, the output wavelength is converted to 400 nm. The pump beam is focused by a cylindrical lens on the sample, while the ASE signal is collected by a lens to the spectrograph.

The ASE property of the $CsPbBr_3$ films (Fig. 6) depicted that the $CsPbBr_3$ films under a low pump power present a broad

Fig. 8 The time resolution of the PL spectrum of the solution (a). The time resolution of the PL spectra of the film with the pump intensities of (b) 10.7 μJ cm^{-2} and (c) 25.0 μJ cm^{-2}.

spontaneous emission (SE) with a peak centered at 529 nm. With increasing pump density, a peak located at 536 nm emerges and quickly becomes dominant. Meanwhile, the FWHM of the emission spectrum narrows sharply, which signifies the transition from an SE process into the ASE regime. The measured emission spectra of the S_D (about 880 nm without solvent annealing) and S_C (about 880 nm with solvent annealing) samples, are shown in Fig. 6(a) and (b), respectively. It can be found that the intensity of the ASE signal is enhanced distinctly under the same pump intensity after solvent annealing (Table S1 in the ESI†). The threshold is decreased from 16.2 μJ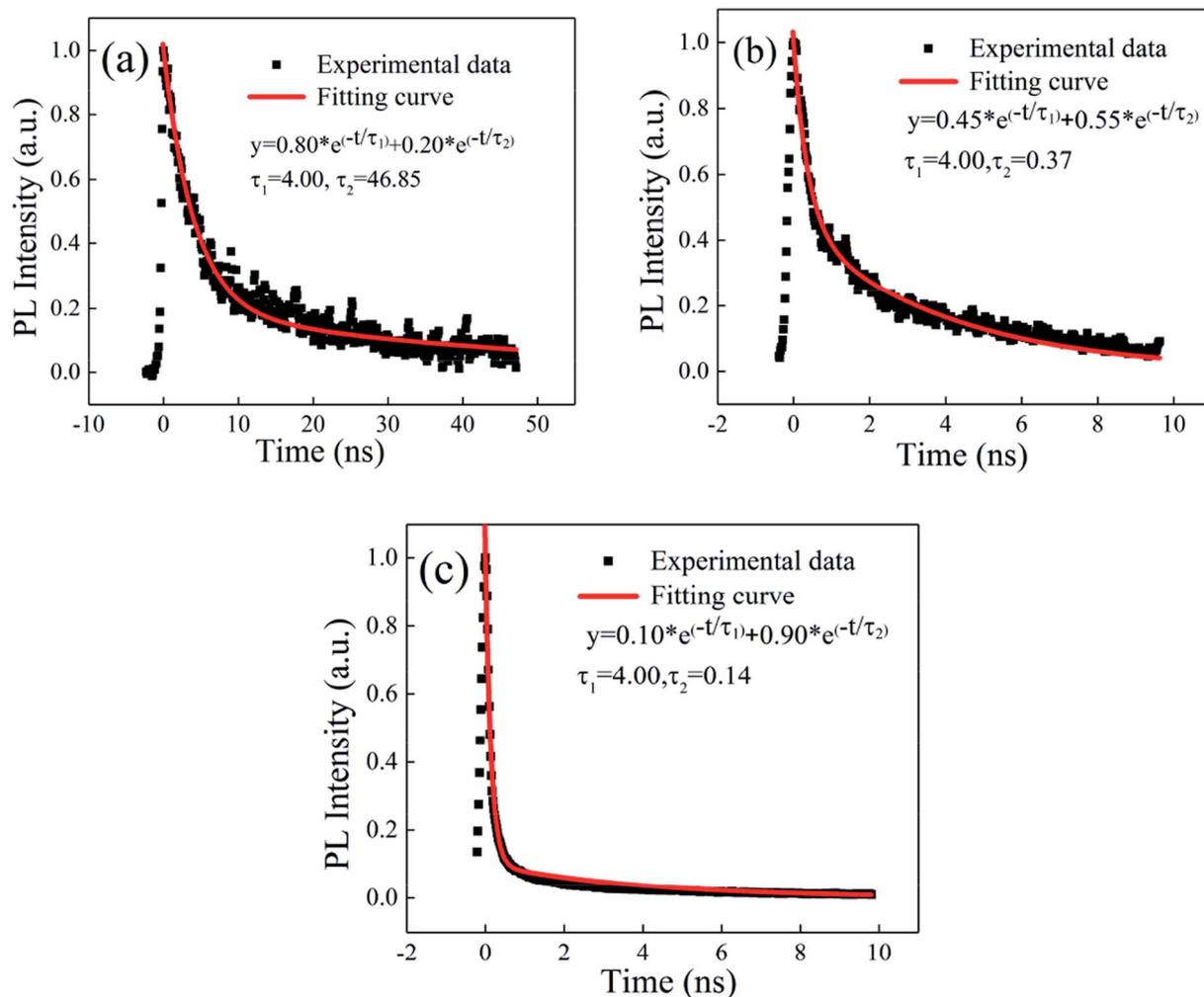 cm^{-2} to 14.1 μJ cm^{-2}. Moreover, the gain coefficient is increased from 112.7 cm^{-1} to 122.7 cm^{-1}, suggesting that solvent annealing can slightly improve the gain coefficient of the CsPbBr$_3$ film. A possible reason for the effect of solvent annealing is the improved surface morphology, which decreases the surface scattering of the film, thus decreasing the threshold and increasing the gain coefficient. The emission spectra of the S_A (about 180 nm with solvent annealing) and S_B (about 500 nm with solvent annealing) samples are shown in Fig. 6(c) and (d). Compared to Fig. 6(c) and (d) with Fig. 6(b), it is obvious that with the increase in the thickness from 180 nm to 880 nm, the intensity of the ASE increases. As a result, the threshold decreases from 18.1 μJ cm^{-2} to 14.2 μJ cm^{-2}, and the gain coefficient increases from 78.5 cm^{-1} to 122.7 cm^{-1}, as shown in Table S2 (ESI†). By comparing Tables S1 and S2 in the ESI,† it can be found that the thickness rather than solvent annealing is the dominant factor that affects the threshold and gain coefficient.

Fig. 7(a) shows the plot of the ASE intensity *versus* the intensity of the pump laser of the S_C sample. Only spontaneous emission occurs under low pump intensity. When the pump intensity increases beyond the threshold, the emission intensity rises rapidly. The threshold of the film is 14.2 μJ cm^{-2}, and the full width at half maximum (FWHM) is 28 nm when the pulse energy is 9.4 μJ cm^{-2}. By further increasing the pulse energy to 45.5 μJ cm^{-2}, the emission FWHM of the CsPbBr$_3$ film decreases to 6 nm. The gain coefficient, a key factor of the gain medium, was measured as 122.7 cm^{-1} by changing the length of the slit, as depicted in Fig. 7(b). The output intensity shows an "S" shape with an increased excitation length. When the stripe length reaches the threshold value where propagation losses are compensated by optical amplification, the PL spectrum starts to show an additional ASE component that increases with the strip length. This is the reason why the output intensity at extremely large stripe lengths will deviate from the first six data.[39,40] The plots of the ASE intensities *versus* the intensity of the pump laser of the S_A, S_B, and S_D samples are also shown in Fig. S2 (ESI†). It can be concluded that the ASE behavior can be optimized greatly through increasing the thickness of the film or performing a solvent annealing treatment.

We measured the emission lifetime using a streak camera (c5680-04/M, Hamamatsu). Fig. 8(a) shows the PL lifetime of the concentrated CsPbBr$_3$ QD solution. The PL lifetime of the CsPbBr$_3$ QD solution contains 4.00 ns and 46.85 ns, which was fitted by a double-exponential function. Fig. 8(b) and (c) show the time domain spectra of the S_C sample. When the pump

intensity increased from 10.7 μJ cm^{-2} to 25.0 μJ cm^{-2}, the measured PL lifetime decreased from 0.37 ns to 0.14 ns. This was caused by the increased proportion of the ASE signal from 55% to 90% due to the increased stimulated radiation probability. The time-resolved PL spectra are shown in Fig. S3 (ESI†).

3 Conclusions

In conclusion, we reported a simple MCDSA method for the preparation of large area homogeneous perovskite CsPbBr$_3$ films using multiple centrifugation cycle deposition and solvent annealing techniques. This method can prepare CsPbBr$_3$ films with a controllable thickness from 180 nm to 880 nm, large area (2.5 cm × 2.5 cm), and low surface roughness (a root mean square is 32 nm). By comparing three samples with different thicknesses (180 nm, 500 nm, and 880 nm), it was shown that the threshold decreased from 18.1 μJ cm^{-2} to 14.2 μJ cm^{-2} and the gain coefficient increased from 78.5 cm^{-1} to 122.7 cm^{-1} with increasing thickness. By comparing a solvent annealed sample to a sample that did not undergo solvent annealing, it was shown that the threshold decreased from 16.2 μJ cm^{-2} to 14.2 μJ cm^{-2}, while the gain coefficient increased from 112.7 cm^{-1} to 122.7 cm^{-1}. The results demonstrated that the threshold and the gain factor parameters can be optimized greatly through increasing the thickness of the sample and performing solvent annealing treatments.

Conflicts of interest

There are no conflicts to declare.

Acknowledgements

References

1 J. H. Li, L. Xu, T. Wang, J. Song, J. Chen, J. Xue, Y. H. Dong, B. Cai, Q. S. Shan, B. N. Han and H. B. Zeng, *Adv. Mater.*, 2017, **29**, 1603885.
2 W. Song, Y. C. Yang, X. J. Kang, L. Wang, L. J. Huang and D. C. Pan, *Chem. Commun.*, 2016, **52**, 7265–7268.
3 H. R. Wang, X. Y. Zhang, Q. Q. Wu, F. Cao, D. W. Yang, Y. Q. Shang, Z. J. Ning, W. Zhang, W. T. Zheng, Y. F. Yan, S. V. Kershaw, L. J. Zhang, A. L. Rogach and X. Y. Yang, *Nat. Commun.*, 2019, **10**, 665.
4 X. Y. Zhang, H. Lin, H. Huang, C. Reckmeier, Y. Zhang, W. C. Choy and A. L. Rogach, *Nano Lett.*, 2016, **16**, 1415–1420.
5 Q. A. Akkerman, V. D'Innocenzo, S. Accornero, A. Scarpellini, A. Petrozza, M. Prato and L. Manna, *J. Am. Chem. Soc.*, 2015, **137**, 10276–10281.
6 L. F. Lv, Y. B. Xu, H. H. Fang, W. J. Luo, F. J. Xu, L. M. Liu, B. W. Wang, X. F. Zhang, D. Yang, W. D. Hu and A. G. Dong, *Nanoscale*, 2016, **8**, 13589–13596.
7 P. Ramasamy, D. H. Lim, B. Kim, S. H. Lee, M. S. Lee and J. S. Lee, *Chem. Commun.*, 2016, **52**, 2067–2070.

8 C. Sun, Y. Zhang, C. Ruan, C. Y. Yin, X. Y. Wang, Y. D. Wang and W. W. Yu, *Adv. Mater.*, 2016, **28**, 10088–10094.

9 J. Z. Song, T. Fang, J. H. Li, L. M. Xu, F. J. Zhang, B. M. Han, Q. S. Shan and H. B. Zeng, *Adv. Mater.*, 2018, **30**, 1805409.

10 H. Wang, Y. Wu, M. Ma, S. Dong, Q. Li, G. Du, H. Zhang and Q. Y. Xu, *ACS Appl. Energy Mater.*, 2019, **2**, 2305–2312.

11 J. Liang, C. X. Wang, Y. R. Wang, Z. R. Xu, Z. P. Lu, Y. Ma, H. F. Zhu, Y. Hu, C. C. Xiao, X. Yi, G. Y. Zhu, H. L. Lv, L. B. Ma, T. Chen, Z. X. Tie, Z. Jin and J. Liu, *J. Am. Chem. Soc.*, 2016, **138**, 15829–15832.

12 J. Z. Chen and N. G. Park, *J. Phys. Chem. C*, 2018, **122**, 14039–14063.

13 J. Ma, H. Wu, J. B. Qiu, J. Wang, Q. Wang, Y. Yang, D. C. Zhou and J. Han, *J. Phys. Chem. C*, 2019, **31**, 1936–1940.

14 Z. H. Wu, J. Wei, Y. N. Sun, J. Wu, Y. F. Hou, P. Wang, N. P. Wang and Z. F. Zhao, *J. Mater. Sci.*, 2019, **54**, 6917–6929.

15 Y. S. Tan, Y. T. Zou, L. Z. Wu, Q. Huang, D. Yang, M. Chen, M. Y. Ban, C. Wu, T. Wu, S. Bai, T. Song, Q. Zhang and B. Q. Sun, *ACS Appl. Mater. Interfaces*, 2018, **10**, 3784–3792.

16 Y. S. Tan, R. Y. Li, H. Xu, Y. S. Qin, T. Song and B. Q. Sun, *Adv. Funct. Mater.*, 2019, **29**, 1900730.

17 R. H. Liu, H. Zhou, Z. N. Song, X. H. Yang, D. J. Wu, Z. H. Song, H. Wang and Y. F. Yan, *Nanoscale*, 2019, **11**, 9302–9309.

18 L. F. Lv, Y. B. Xu, H. H. Fang, W. J. Luo, F. J. Xu, L. M. Liu, B. W. Wang, X. F. Zhang, D. Yang, W. D. Hu and A. G. Dong, *Nanoscale*, 2016, **8**, 13589–13596.

19 Y. P. Fu, H. M. Zhu, C. S. Constantinos, Q. Ding, J. Wang, G. K. Mercouri, X. Y. Zhu and J. Song, *ACS Nano*, 2016, **10**, 7963–7972.

20 J. Pan, P. S. Smritakshi, M. Banavoth, D. Ibrahim, W. Peng, R. P. Manas, J. K. Liu, L. F. Sinatra, N. T. Alyami, C. Zhao, E. Alarousu, T. K. Ng, S. O. Boon, M. B. Osman and F. M. Omar, *J. Phys. Chem. Lett.*, 2015, **6**, 5027–5033.

21 Y. Wang, X. M. Li, J. Z. Song, L. Xiao, H. B. Zeng and H. D. Sun, *Adv. Mater.*, 2015, **27**, 7101–7108.

22 B. Conings, L. Baeten, C. D. Dobbelaere, J. D'Haen, J. Manca and H. G. Boyen, *Adv. Mater.*, 2014, **26**, 2041–2046.

23 M. D. Xiao, F. Z. Huang, W. C. Huang, Y. Dkhissi, Y. Zhu, J. Etheridge, G. W. Angus, U. Bach, Y. B. Cheng and L. Spiccia, *Angew. Chem.*, 2014, **126**, 10056–10061.

24 N. J. Jeon, J. H. Noh, Y. C. Kim, W. S. Yang, S. C. Ryu and S. Seok, *Nat. Mater.*, 2014, **13**, 897–903.

25 Y. C. Ling, Y. Tian, X. Wang, M. K. Javon, P. O. Fernando, Y. J. Du, L. Tan, K. Hanson, B. W. Ma and H. W. Gao, *Adv. Mater.*, 2016, **28**, 8983–8989.

26 Y. K. Chih, J. C. Wang, R. T. Yang, C. C. Liu, Y. C. Chang, Y. S. Fu, W. C. Lai, P. Chen, T. C. Wen, Y. C. Huang, C. S. Tsao and T. F. Guo, *Adv. Mater.*, 2016, **28**, 8687–8694.

27 J. Chen, Y. P. Fu, L. Samad, L. Dang, Y. Z. Zhao, S. H. Shen, L. J. Guo and J. Song, *Nano Lett.*, 2017, **17**, 460–466.

28 M. Z. Liu, M. B. Johnston and H. J. Snaith, *Nature*, 2013, **501**, 395–398.

29 J. Chen, D. J. Morrow, Y. P. Fu, W. H. Zheng, Y. Z. Zhao, L. Dang, M. J. Stolt, D. D. Kohler, X. X. Wang, K. J. Czech, M. P. Hautzinger, S. H. Shen, L. J. Guo, A. L. Pan, J. C. Wright and J. Song, *J. Am. Chem. Soc.*, 2017, **139**, 13525–13532.

30 Y. C. Ling, L. Tan, X. Wang, Y. Zhou, Y. Xin, B. W. Ma, K. Hanson and H. W. Gao, *J. Phys. Chem. Lett.*, 2017, **8**, 3266–3271.

31 L. Ji, X. Z. Zhang, T. Zhang, Y. F. Wang, F. Wang, Z. Q. Zhong, Z. D. Chen, Z. W. Xiao, L. Chen and S. B. Li, *J. Mater. Chem. A*, 2019, **7**, 9154.

32 F. Wang, T. Zhang, Y. F. Wang, D. T. Liu, P. Zhang, H. Chen, L. Ji, L. Chen, Z. D. Chen, J. Wu, X. Liu, Y. B. Li, Y. F. Wang and S. B. Li, *J. Mater. Chem. A*, 2019, **7**, 12166.

33 P. Zhang, T. Zhang, Y. F. Wang, D. T. Liu, H. Xu, L. Chen, Y. B. Li, J. Wu, Z. D. Chen and S. B. Li, *J. Power Sources*, 2019, **439**, 227091.

34 D. Liu, H. L. Zheng, L. Ji, H. Chen, Y. F. Wang, P. Zhang, F. Wang, J. Wu, Z. Chen and S. B. Li, *J. Power Sources*, 2019, **441**, 227161.

35 Y. Kim, E. Yassitepe, C. Riccardo, G. Walters, X. W. Gong, P. Kanjianaboos, A. F. Nogueira and E. H. Sargent, *ACS Appl. Mater. Interfaces*, 2015, **7**, 25007–25013.

36 J. Y. Kim, V. Adinolfi, B. R. Sutherland, O. Voznyy, S. J. Kwon, T. W. Kim, J. Kim, H. Ihee, K. Kemp, M. Adachi, M. J. Yuan, L. kramar, D. Zhitomirsky, S. Hoogland and E. H. Sargent, *Nat. Commun.*, 2015, **6**, 7772.

37 S. B. Sun, D. Yuan, Y. Xu, A. F. Wang and Zh. T. Deng, *ACS Nano*, 2016, **10**, 3648–3657.

38 X. M. Li, D. J. Yu, F. Cao, Y. Gu, Y. Wei, Y. Wu, J. Z. Song and H. B. Zeng, *Adv. Funct. Mater.*, 2016, **26**, 5903–5912.

39 P. Liu, X. X. He, J. H. Ren, Q. Liao, J. N. Yao and H. B. Fu, *ACS Nano*, 2017, **11**, 5766–5773.

40 S. Yakunin, L. Protesescu, F. Krieg, M. I. Bodnarchuk, G. Nedelcu, M. Humer, G. D. Luca, M. Fiebig, W. Heiss and M. V. Kovalenko, *Nat. Commun.*, 2015, **6**, 8056.